Increasing the effect of annonacin using nanodiamonds to inhibit breast cancer cells growth in rats (Rattus norvegicus)-Induced breast cancer

by Hartono Hartono

Submission date: 21-Jun-2023 01:12PM (UTC+0100)
Submission ID: 209266210
File name: 7.pdf (2.84M)
Word count: 8422
Character count: 44970

Heliyon 8 (2022) e11418

Contents lists available at ScienceDirect

Heliyon

journal homepage: www.cell.com/heliyon

Research article

Increasing the effect of annonacin using nanodiamonds to inhibit breast cancer cells growth in rats (*Rattus norvegicus*)-Induced breast cancer

Firli Rahmah Primula Dewi [a,*], Nadia Shoukat [a], Na'ilah Insani Alifiyah [a], Sri Puji Astuti Wahyuningsih [a], A'liyatur Rosyidah [b], Muhammad Darwin Prenggono [c], Hartono Hartono [d]

[a] Department of Biology, Faculty of Science and Technology, Universitas Airlangga, Surabaya 60115, Indonesia
[b] Research Center for Vaccine and Drug, National Research and Innovation Agency (BRIN), Bogor 16911, Indonesia
[c] Division of Hematology, Medical Oncology, Ulin General Hospital, Banjarmasin 70714, Indonesia
[d] Department of Biology, Faculty of Mathematics and Natural Sciences, Universitas Negeri Makassar, Makassar 90224, Indonesia

ARTICLE INFO

Keywords:
Annonacin
Breast cancer
Nanodiamonds
PI3K
ROS

ABSTRACT

Background: Annonaceous acetogenins have been reported to have anti-cancer properties but low viability. In this study, we aimed to investigate the potency of nanodiamonds to be employed as a carrier of annonacin to help increase its viability and inhibit the growth of breast cancer cells.

Methods: The annonacin was coupled with nanodiamond and characterized using UV-Vis spectrophotometer, FTIR, SEM, and PSA, and determined their stability and drug release. A cell growth inhibition assay and cell migration assay was performed using the breast cancer MCF7 and T747D cell lines, and in vivo analysis was performed in rats (*Rattus norvegicus*). MCF7 and T747D cells were treated with 12.5 μg/mL annonacin coupled with nanodiamonds for 24 and 48 h and further analyzed by MTT, cell migration, and reactive oxygen species (ROS) assays. Twenty-five female rats were divided into five groups. Breast cancer was induced using two intraperitoneal doses of N-nitroso-N-methylurea (NMU) (50 and 30 mg/kg body weight). Annonacin coupled with nanodiamonds was administered by intraperitoneal injection (17.5 mg/kg body weight) for 5 weeks, one injection per 3 days.

Results: Administration of annonacin coupled with nanodiamonds significantly reduced MCF7 cell growth and reactive oxygen species (ROS) levels. The in vivo study showed that administration of annonacin coupled with nanodiamonds significantly reduced PI3KCA levels and increased p53 expression, reduced cancer antigen-15-3 (CA-15-3) levels in serum, increased caspase-3 expression, reduced Ki-67 levels, and reduced the thickness of the mammary ductal epithelium.

Conclusions: Collectively, this study demonstrated the effectiveness of nanodiamonds as a carrier of annonacin to inhibit breast cancer cell growth through inhibition of the PI3K/Akt signaling pathway.

1. Introduction

Cancer is a leading cause of morbidity and mortality worldwide. The rate of annual decline in overall cancer mortality doubled from 2.4% (2009–2013) to 5% (2014–2018). Despite the trend of declining cancer mortality, 1,898,160 new cancer cases and 608,570 cancer deaths are projected to occur in the United States in 2021 (Siegel et al., 2021). Breast cancer is one of the most common cancers among women, worldwide (Abd-Rabou et al., 2017). In the United States, the estimated new cases of breast cancer in 2021 were 284,200, and the mortality rate of breast cancer patients was estimated to be about 15.5% of the total breast cancer cases (Siegel et al., 2021).

During normal metabolic processes, the body produces oxidants known as free radicals. Although oxidants are continuously produced, cells have an antioxidant system, such as enzymes that remove free radical molecules. This process is important because the availability of excess oxidants or impairment of the antioxidant system causes oxidative stress that destroys DNA, proteins, lipids, and carbohydrate molecules, thus accelerating cancer development (Coughlin, 2018). Oxidative stress accelerates cancer cell proliferation, angiogenesis, and metastasis by

* Corresponding author.
E-mail address: firli.rahmah@fst.unair.ac.id (F.R.P. Dewi).

https://doi.org/10.1016/j.heliyon.2022.e11418
Received 20 May 2022; Received in revised form 21 September 2022; Accepted 31 October 2022

causing genomic instability activation of various signaling pathways involved in cancer cell promotion or activation of various oncogenes and suppressor genes (Liou and Storz, 2010).

The level of reactive oxygen species (ROS) play an important role in carcinogenesis and affect multiple biological processes, such as cell proliferation, differentiation, inflammation, cell survival, and resistance to apoptosis. ROS can lead to lipid peroxidation, which is often monitored by measuring malondialdehyde (MDA) levels. ROS-sensitive signaling pathways, including the MAPK/ERK, NF-κB, and PI3K/Akt pathways, are often elevated in many types of cancers (Liou and Storz, 2010). ROS generation during estrogen metabolism and other potential mammary carcinogens were shown to activate the PI3K signaling pathway (Burdick et al., 2003; Park et al., 2009).

Annonacin is an acetogenin produced by the members of the Annonaceae family. It has the potential to prevent cell division by arresting the cell cycle, thereby inhibiting cell proliferation. In T24 bladder cancer cells, annonacin induced cell cycle arrest and caused cytotoxicity in a Bax and caspase-3 related pathway (Yuan et al., 2003). In cancers induced by N-nitroso-N-methylurea (NMU), annonacin was able to arrest the cell cycle at the G1 phase by stimulating the p21 protein (Wahab et al., 2018). Furthermore, the compound was reported to inhibit the proliferation of MCF-7 breast cancer cells by decreasing the expression of ER, cyclin D1, and Bcl2 (Qazi et al., 2018). Despite its potential as an anti-cancer agent, a pharmacokinetics study showed that annonacin has low bioavailability and solubility (Gutierrez et al., 2020), and a low ability to cross the blood-brain barrier (Chan et al., 2019). Gutirezz et al. (2020) reported that the use of supramolecular polymer micelles (SMPM) as nanocarriers for annonacin in a drug delivery system increased its bioavailability and solubility; thereby demonstrating that the use of a carrier improves the bioavailability of annonacin.

A nanodiamond is a nanoparticle of an allotrope of carbon, usually with a diameter ranging from 2 to 100 nm. Recently, it has been used as a carrier to deliver drugs to specific target cells. Nanodiamonds have attracted considerable attention in therapies because they are safe, effective, produce a strong response, and cannot be recognized by the immune system (El-Say, 2011; Tsai et al., 2016). A nanodiamond has unsaturated bonds of carbon on its surface and extraordinary sorption and chemical linking capabilities that interact with molecules of interest (Tsai et al., 2016; Chauhan et al., 2020). Several studies have shown good results when nanodiamonds were used as drug carriers in cancers (Wei et al., 2019). The conjugation of nanodiamonds with doxorubicin decreases tumor growth, overcomes drug efflux, and increases apoptosis of cancer cells (Chow et al., 2011). Due to their biocompatibility property, possibility nanodiamonds can be used as a carrier to deliver annonacin to breast cancer cells, thus enhancing its bioavailability and anti-cancer properties. Despite this possibility, to the best of our knowledge, no studies have investigated the possibility of using nanodiamonds as a carrier of annonacin. Therefore, this study aimed to investigate the potency of nanodiamonds as carriers of annonacin to inhibit the growth of breast cancer.

2. Material and methods

2.1. Conjugation of annonacin with nanodiamonds

Carboxyl-modified nanodiamond (ND) solution (1 mg/mL) (TCI, N1084) was sonicated for 5 min using a sonicator. N-(3-dimethylaminopropyl)-N-ethylcarbodiimide hydrochloride (EDC, 8.35 μg) and sulfo-N-hydroxysulfosuccinimide (NHS, 9.5 μg) were dissolved in dH_2O, and added to the ND suspension. Thirty minutes after stirring, 200 μg of methyl polyethylene glycol (mPEG) was added to the activated ND solution, and the mixture was stirred overnight at 25 °C. The mixture was then centrifugated at 14,000 rpm for 2 h, and the pellet was collected and dispersed in NaOH (2.5 mM) by sonication for 5 min. Next, annonacin (2 mg/mL) dissolved in DMSO was added, and the mixture was incubated overnight using a rotating shaker at RT to allow the binding of annonacin to the surface of the nanodiamonds. Finally, the nanodiamond + annonacin complex was purified from the other substances by centrifugation at 14,000 rpm for 2 h and washing the pellet with dH_2O. The compound loading efficiency (CLE) was calculated using the following equation:

CLE = (compound added initially − compound in the supernatant after centrifugation) / (compound added initially) x 100%

The absorbance values of annonacin before and after adsorption were measured using a UV-vis spectrophotometer (Thermo Scientific Multiskan Go) at λ 250–350 nm.

2.2. Characterization of annonacin-nanodiamond complex

The annonacin-nanodiamond complex was characterized by scanning electron microscopy (SEM), Uv-vis spectrophotometry, Fourier transform-infrared (FT-IR) spectroscopy, and zeta potential analysis. The absorbance of annonacin before and after conjugation was measured using UV-Vis spectrophotometer (Thermo Scientific Multiskan Go) at λ 290 nm to determine drug-loading efficiency. The FT-IR spectroscopy measurements of annonacin (AN), nanodiamonds (ND), and annonacin nanodiamond (NDAN) complex was performed using an FT-IR spectrometer (PerkinElmer FT-IR Spectrometer Spectrum Two) in the 4000-400 cm-1 range. The nanodiamond powders were placed in a diamond chamber and the spectra were recorded immediately. For each sample, the signal obtained from the blank chamber was subtracted as a background. The spectral data were compared to those in the database to determine the functional groups in each sample. The zeta potential of the nanodiamonds was measured using a particle size analyzer (Horiba SZ-100).

2.3. Stability of annonacin-nanodiamond complex in different media

The stability of nanodiamonds during interaction with DMEM (Dulbecco's Modified Eagle Medium), 10% fetal bovine serum (FBS), and complete DMEM media were analyzed by measuring their zeta potential using a particle size analyzer (Horiba SZ-100). The experiments were performed by dispersing the nanodiamonds at a concentration of 200 μg/mL in different media. After incubation, the samples were centrifuged for 10 min at 12,000 g. The pellets thus obtained were suspended in distilled water, shaken, sonicated for 10 min, and resuspended. The centrifugation was repeated thrice. The final aggregates were resuspended in distilled water (Hemelaar et al., 2017).

2.4. Drug release study of the annonacin-nanodiamond complexes

To construct the calibration curve of annonacin, concentrations of 1:9 DMSO-PBS and annonacin were prepared at 0.0625–8 mg/ml. A calibration curve was plotted using the absorbance values at λ = 285 nm using a UV-vis spectrophotometer (Varioskan™ LUX multimode microplate reader). For the drug release study, annonacin nanodiamonds were tested for sustained release capacity in physiological buffer media according to the method of Roy et al. (2018), with some modifications. Firstly, 0.5 ml of annonacin nanodiamond solution (40 mg/mL) was placed into a dialysis bag filled with 50 ml dissolution solution consisting of PBS pH 7.4 and 0.1% Tween 20. The sample was dialyzed against the buffer solution at 37 °C at 150 rpm. At each time point, 1000 μL of the solution was removed from the tank, and an equal amount of fresh buffer was replaced. The final drug concentrations of the collected samples were determined using a UV-Vis spectrophotometer (Varioskan™ LUX Multimode Microplate Reader) at λ = 285 nm.

2.5. 3-(4,5-Dimethylthiazol-2-yl)-2,5-diphenyl-2H-tetrazolium bromide (MTT) assay

MCF-7 and T47D cells (5,000/well) were seeded in a 96-well plate. After 24 h, the cell groups were treated with the following reagents according to indicated time courses:

CTL group: MCF7 cells administered with dimethyl sulfoxide (DMSO)
ND group: MCF7 cells administered with nanodiamonds
AN group: MCF7 cells administered with 12.5 μg/mL of annonacin
NDAN group: MCF cells administered 12.5 μg/mL annonacin coupled with nanodiamonds

After each indicated time course, 10 μl of 12 mM MTT solution was added to each well, followed by 3 h of incubation, and the reaction was stopped by adding 100 μl of STOP solution. The samples were mixed thoroughly, and absorbance was measured at 570 nm (Dewi et al., 2021). To determine the inhibitory concentration (IC)-50, free annonacin and annonacin coupled with nanodiamonds were added at several doses (0; 0.4; 0.8; 1.5; 3; 6; 12.5; 25; 50; 100; 200) μg/mL to MCF7 and T47D cells, and the cells were incubated for 48 h.

2.6. Cell migration and motility assay

Cell migration and motility were evaluated using a wound-healing assay. Briefly, MCF7 and T47D cells were seeded at a density of 8×10^4 cells/well in 6-well plates and cultivated for 48 h. Each disc was artificially wounded by creating a scratch on the cell monolayer using a 10 μl plastic pipette tip. The cells were treated according to the indicated treatment groups and cultured for another 48 h. Images of scratch wounds were captured using a Nikon inverted microscope. Measurements of wound width were subtracted from those of the wound width at time zero to obtain net wound closure. The percentage of wound closure were then calculated.

2.7. ROS level measurement

ROS levels were measured using an ROS assay kit (SolarBio China #CA1410). Briefly, the cell culture medium was removed, and 2′,7′-dichlorofluorescein diacetate (DCFH-DA) (10 μmol/L) until the cells were fully covered. The cells were then incubated at 37 °C for 20 min and were washed with serum-free culture medium to remove DCFH-DA completely. Next, the cells were observed under a confocal laser scanning microscope (Olympus) using an FITC fluorescence spectrum at an excitation wavelength of 488 nm and emission wavelength of 525 nm.

2.8. Animal model experimental design and ethics

All procedures involving animal models were approved by the Animal Care and Use Committee of the Faculty of Animal Health, Universitas Airlangga (No. 2. KE.046.04.2021). Twenty-five female rats (species *Rattus novergicus*, 4–8 weeks old, 250–300 g weight) were placed in plastic cages covered by a wire gauze; 5 rats of each group were kept as 2–3 rats/cage. The rats were maintained under standard conditions in a 12 h dark-light cycle. Before commencing the treatments, the rats were acclimatized for two weeks, and then grouped into five groups.

Normal control group (CTL): normal control, injected with buffer saline.
Negative control group (K-): injected with NMU in buffer saline.
Nanodiamond group (ND): injected with NMU and nanodiamonds.
Annonacin group (AN): injected with NMU and annonacin.
Annonacin coupled with nanodiamonds (NDAN): injected with NMU and annonacin coupled with nanodiamonds.

Breast cancer was induced by two intraperitoneal injections of NMU. The first NMU dose used for injection was 50 mg/kg body weight and the second was 30 mg/kg body weight. Breast cancer formation was assessed by palpitation, and when the breast cancer was formed, the rats were intraperitoneally injected with the respective substances mentioned above. The treatment was carried out for 5 weeks, with one injection per 3 days. The concentration of annonacin (AN) and annonacin coupled with nanodiamonds for each injection was 17.5 mg/kg body weight. Annonacin was purchased from Anhui Minmetals Development Ltd. (China).

2.9. Serum collection

After the final day of treatment, the rats were sacrificed under ketamine anesthesia (Tsai et al., 2016). Blood was collected from the left ventricle using a 26G injection needle and collected in 5 ml microtubes. To isolate serum from the blood, the blood was allowed to stand for 2 h, centrifuged at 1000 rpm for 5 min, and the upper phase was collected.

2.10. Protein isolation

Mammary gland tissue was isolated from the sacrificed rats, cleaned using buffer saline, placed in a mortar containing liquid nitrogen, and crushed using a pestle. The ground mammary gland tissue was filtered using a 200 μm filter, and the suspension was centrifuged at 2000 rpm for 5 min. The pellets were collected, NH_4Cl was added, and the mixtures were centrifuged at 2000 rpm for 5 min. The procedure was repeated to obtain white pellets, which were then suspended in buffer saline and sonicated at 2-kHz for 20 s (6 times) under ice-cold conditions. The homogenates were centrifuged at 2500 rpm for 5 min, and the supernatants were collected and stored at -20 °C for further use.

2.11. Determination of the levels of malondialdehyde (MDA) in serum

The serum levels of MDA were measured using a spectrophotometric assay (Solarbio, BC0025). The kit contained an extraction reagent, R1 solution, R2 powder, and R3 solution. MDA working reagent was prepared by adding 15 mL of R1 to R2, and the mixture was heated in a water bath at 70 °C. In each sample test tube, 300 μL of the MDA working reagent, 100 μL of serum, and 100 μL of R3 were added. In addition, in the blank tube, 300 μL of MDA working reagent, 100 μL distilled water, and 100 μL of R3 were added. All the tubes were closed tightly and incubated at 100 °C for 60 min. After incubation, the tubes were cooled in an ice bath and centrifuged at 10,000 g for 10 min at room temperature to remove insoluble materials. Absorbance of the supernatants was measured at 450, 532, and 600 nm. The concentration of MDA was measured using the following equation provided by the manufacturer:

$$\text{MDA (nmol/ mL)} = (12.9 \times(\Delta A532\text{-}\Delta A600)\text{-}2.58\times\Delta A450) \times V \div Vs = 5\times (12.9\times(\Delta A532\text{-}\Delta A600)\text{-}2.58\times\Delta A450)$$

2.12. Enzyme-linked immunosorbent assay (ELISA)

The levels of ERBB2 (Finetest, ER1910), p53 (Finetest, ER0394), PI3KCA (Finetest, ER0606) and CA-15-3 (Finetest, ER0789) were determined by ELISA. The levels of ERBB2, p53, and PI3KCA were measured from tumor tissue proteins, while CA-15-3 was measured from serum proteins. Briefly, 50 μL of standards (5000, 2500, 1000, 500, 250, 0 pg/mL) were added to each well, and the plate was shaken gently. Next, 50 μL of PBS (pH 7.0–7.2) was added to the blank control and, 5 μL of balance solution was added to 50 μL of the samples. In each well, 50 μL of the conjugate was added, except in the control well. The plate was then covered and incubated for 60 min at 37 °C The plate was washed with the diluted solution and air-dried. Subsequently, substrate A and substrate B were added to each well, including the control, and the plate was incubated for 15–20 min at 37 °C. Next, 50 μL of stop solution was added and mixed. Absorbance was measured at a wavelength of 450 nm.

2.13. Hematoxylin eosin (H-E) staining and epithelial thickness measurement

Briefly, 4-μm thick paraffin-embedded tissue blocks were sectioned onto slides and deparaffinized. The slides were then placed overnight in an oven and deparaffinized. The slides were then stained with hematoxylin solution for 10 min, washed with running water, and incubated

with acidic ethanol (1% HCl in 70% ethanol) for 5 s. After that, the slides were incubated with eosin staining for 5 min, washed, and incubated in alcohol series (ethanol 70% - ethanol absolute), followed by a series of xylol I and xylol II. The slides were mounted using Entellan mounting medium and observed under a microscope (Nikon, Japan). Epithelial thickness was measured using ImageJ software.

2.14. Immunohistochemical staining and analysis

Immunohistochemical staining was performed according to the manufacturer's guidelines (Finetest, IHC0007). Briefly, 4-μm thick paraffin-embedded tissue blocks were sectioned onto slides, and the sections were deparaffinized. The sections were then blocked for 1 h with blocking serum at 37 °C. The slides were incubated with primary antibodies against Ki-67 (Invitrogen, MA5-14520) and caspase-3 (Invitrogen, PA1-29157) overnight at 4 °C, washed, and incubated using poly-HRP goat anti-rabbit IgG as a secondary antibody at room temperature for 1 h. Color was developed using 3,3'-diaminobenzidine tetrahydrochloride for 2–10 min, and the sections were counterstained with hematoxylin. Images were acquired using a Nikon microscope (Tokyo, Japan) and digitally processed using ImageJ software to measure the percentage of cells exhibiting positive staining of Ki-67 and caspase-3.

2.15. Statistical analysis

Statistical analysis was performed using PRISM software with one-way analysis of variance (ANOVA). $P < 0.05$ was considered statistically significant.

3. Results

3.1. Characterization of annonacin-nanodiamond complex

The conjugation of annonacin to nanodiamonds was investigated using SEM imaging, Uv-Vis spectrophotometry, and FT-IR. The results showed that the size of the complex was approximately 150–300 nm, indicating successful conjugation (Figure 1A). The Uv-Vis results showed that the absorbance of annonacin at 290 nm before conjugation with nanodiamonds was 3.56, and the absorbance after conjugation was 0.93, indicating that the drug-loading efficiency was approximately 74% (Figure 1B). Figure 1C shows the results of FT-IR characterization of annonacin (AN), nanodiamond (ND), and annonacin-nanodiamond complex (NDAN) used in this study. The nanodiamonds exhibited strong peaks at 2970, 1738, 1365, and 1055 cm^{-1}, corresponding to CH_3 asymmetric stretching, C=O stretching, C–O stretching, and C–O stretching, respectively (Petit and Puskar, 2018). The annonacin spectra exhibited strong signals at 3304, 2922, 1743, and 1011 cm^{-1}, corresponding to O–H stretching, C–H stretching, C=O stretching, and C=O, respectively. These spectra were not present in the nanodiamond spectra. The FT-IR spectra of the annonacin-nanodiamonds clearly demonstrate the presence of the characteristic features of the corresponding annonacin spectra at 3371, 1782, and 1026 cm^{-1}. The shifted wavenumber might have been because of absorption of annonacin into the nanodiamonds. Characteristic bands of both annonacin and nanodiamonds appeared in the FT-IR spectra of the annonacin-nanodiamond complex, confirming successful absorption of annonacin on the nanodiamonds.

The zeta potential of the nanodiamonds was -81.1 ± 0.6 mV. The adsorption of annonacin caused the zeta potential on nanoparticles to be increased to -65.8 ± 0.1 mV (Table 1).

The stability of annonacin coupled with nanodiamond particles in DMEM was evaluated to compare the stability of the complex in different media. Zeta potential analysis showed that the zeta potential of nanodiamonds in DMEM was -57.5 ± 0.2 mV. The adsorption of annonacin caused the zeta potential of the nanoparticles to be reduced to -66.5 ± 0.2 mV. In 10% FBS, the zeta potential of nanodiamonds was -53.1 ± 0.1 mV, and the adsorption of annonacin resulted in the zeta potential to be reduced to -67.4 ± 0.2 mV. In complete DMEM, the zeta potential of nanodiamonds was -57.2 ± 0.5 mV, and the adsorption of annonacin

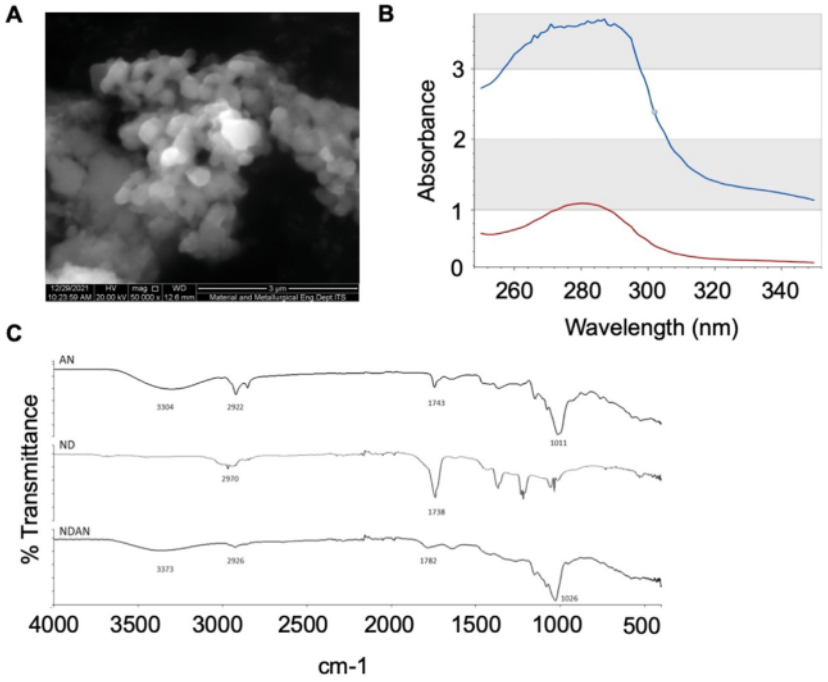

Figure 1. (A) Imaging of annonacin-nanodiamond complex by using SEM (magnification 40.000x). (B) Uv-vis of annonacin before and after adsorption. (C) Fourier transform infrared spectroscopy of annonacin, nanodiamond, and annonacin nanodiamond.

caused the zeta potential to be slightly reduced to -58.6 ± 0.4 mV (Table 2).

3.2. Release of annonacin from nanodiamonds

Sustained drug release of annonacin-nanodiamond complex was determined using the dialysis method in phosphate-buffered saline (PBS). To measure the drug released outside the dialysis bag, samples were taken at intervals up to 72 h. The results are shown in terms of the amount of annonacin released from the nanodiamond (in mg/mL) relative to that of the initial drug load. The release assay demonstrated a biphasic behavior, with the release of an initial burst of annonacin for 6 h, followed by sustained release for up to 72 h. After 42 h, annonacin was released slowly at 37 °C. The annonacin release profile in aqueous solution suggested that the nanodiamond complex was stable (Figure 2).

3.3. 50% inhibitory concentration (IC_{50}) and effect of annonacin coupled with nanodiamonds on growth of MCF7 and T47D cells

In MCF7 cells, the IC_{50} of free annonacin was 21.1 μg/mL, while the IC_{50} of annonacin coupled with nanodiamonds was 14.41 μg/mL (Figure 3A-B). In T47D cells, the IC_{50} of free annonacin was 69.88 μg/mL, and the IC_{50} of annonacin coupled with nanodiamonds was 22.72 μg/mL (Figure 3C-D). The viability of MCF7 cells was significantly reduced in annonacin-nanodiamond complex-treated cells at 24 h compared to that in the cells of CTL group ($P < 0.05$). At 48 h after treatment, the cell viability in both the AN and NDAN groups was significantly reduced compared to that in the CTL group ($P < 0.05$). However, there was no significant difference in cell growth between the AN and NDAN groups after 48 h of treatment (Suppl. Figure 1).

3.4. Effect of annonacin coupled with nanodiamonds on cells migration and motility

To determine the effect of annonacin coupled with nanodiamonds on cell migration and motility, we performed a wound-healing assay using MCF7 and T47D cells. The results showed that migration and motility of MCF7 and T47D cells in the NDAN-12.5 group were significantly slower than those in the AN-12.5 group ($P < 0.05$). The % wound closure of MCF7 cells in AN-12.5 and NDAN-12.5 group was 76.86 ± 3.2% and 54.2 ± 4.0%, and in T47D cells was 41.97 ± 16.16 and 20.93 ± 11.76%, while in CTL group it was 89.95 ± 3.25% and 94.138 ± 4.63%, respectively. The increased dose of AN to 75 μg/mL significantly reduced the wound closure percentage compared to the lower dose, however there is no significant difference of wound closure percentage between AN-75 group than those in NDAN-75 group (Figure 4).

3.5. Effect of annonacin coupled with nanodiamonds on ROS levels in MCF7 cells

To investigate the antioxidant activity of annonacin coupled with nanodiamonds, we measured the ROS levels in MCF7 cells. High levels of ROS promote tumor development and metastasis. Treatment with annonacin coupled with nanodiamonds for 24 h significantly ($P < 0.05$) reduced ROS levels in MCF7 cells than in cells of the CTL group. The ROS levels in the NDAN group were significantly ($P < 0.05$) lower than those in the AN group (Figure 5).

Table 1. Zeta potential value of annonacin-nanodiamond complex in water.

Sample	Zeta potential value (mV)
Nanodiamonds	-81.1 ± 0.6
Annonacin-nanodiamond complex	-65.8 ± 0.1

Table 2. Zeta potential value of annonacin-nanodiamond complex in different media.

Sample	Zeta potential value (mV)		
	DMEM	10% FBS	Complete DMEM
Nanodiamonds	-57.5 ± 0.2	-53.1 ± 0.1	-57.2 ± 0.5
Annonacin-nanodiamond complex	-66.5 ± 0.2	-67.4 ± 0.2	-58.6 ± 0.4

3.6. Effect of annonacin coupled with nanodiamond on MDA level in breast cancer-induced rats

To investigate the lipid peroxidation activity of ROS in vivo, we measured MDA levels in the serum of breast cancer-induced rats. MDA is the most common biomarker of oxidative stress in many health conditions, including cancer. Annonacin coupled with nanodiamond administration significantly ($P < 0.05$) reduced MDA levels in the serum of breast cancer-induced rats compared to those in the CTL (-) group. MDA levels in the AN and NDAN groups were not statistically different, as the level of MDA in both groups was similar to that in the NC group (Figure 6).

3.7. Effect of annonacin coupled with nanodiamond on the P13K/Akt signaling pathway in breast cancer-induced rats

The P13K/Akt signaling pathway is ROS-sensitive. First, we examined ERBB2 levels as an upstream molecule of PI3K. ERBB2 levels were not significantly different between groups (Figure 7A). Annonacin coupled with nanodiamond administration in breast cancer-induced rats significantly ($P < 0.05$) reduced PI3KCA/P110α (a subunit of PI3K) expression compared to that in the CTL (-) group. The levels of PI3KCA in the AN and NDAN groups were significantly different ($P < 0.05$) (Figure 7B). In contrast, the administration of annonacin coupled with nanodiamond significantly ($P < 0.05$) increased P53 (a tumor suppressor protein) expression compared to that in the CTL (-) group. The level of P53 in the AN and NDAN groups were significantly different ($P < 0.05$) (Figure 7C).

3.8. Effect of annonacin coupled with nanodiamond on serum levels of cancer antigen 15–3 (CA-15-3) in rats with breast cancer

To investigate the potential of annonacin coupled with nanodiamond to prevent breast cancer metastasis, we measured the serum levels of CA-15-3, a marker for breast cancer metastasis. The serum level of CA-15-3 is used as a marker to monitor metastatic breast cancer patients undergoing treatment and for the detection of tumor recurrence (Prabasheela and Arivazhagan, 2011; Hashim, 2013; Keshaviah et al., 2007). Annonacin coupled with nanodiamond administration significantly ($P < 0.05$) reduced CA-15-3 levels in the serum of breast cancer-induced rats compared to those in the CTL (-) group. The CA-15-3 levels in the AN and NDAN groups were not statistically different, as the level of CA-15-3 in both groups was already below that in the NC group (Figure 8).

3.9. Effect of annonacin coupled with nanodiamonds on proliferation and apoptosis in rats with breast cancer

To investigate the effect of annonacin coupled with nanodiamonds on proliferation and apoptosis in breast cancer induced in rats, we performed immunohistochemical staining for Ki-67 (proliferation marker) and caspase-3 (apoptosis marker). We also measured the thickness of the mammary ductal epithelium, which was thickened as a consequence of cell proliferation and apoptosis. Administration of annonacin coupled with nanodiamonds significantly ($P < 0.05$) reduced the percentage of cells displaying positive Ki-67 staining compared to that in the CTL(-) group (Figure 9). The percentage of cells showing positive Ki-67 staining was significantly different between the AN and NDAN groups ($P < 0.05$). In contrast, the administration of annonacin coupled with nanodiamonds

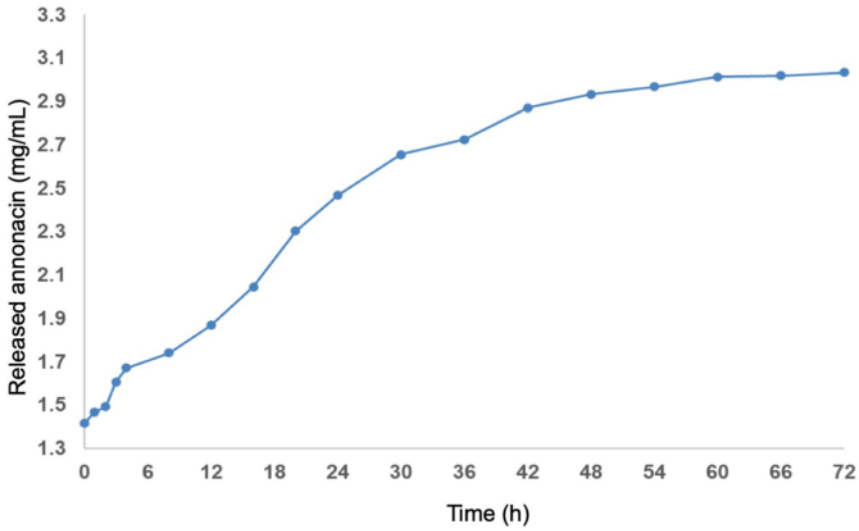

Figure 2. In vitro annonacin release from nanodiamond complex.

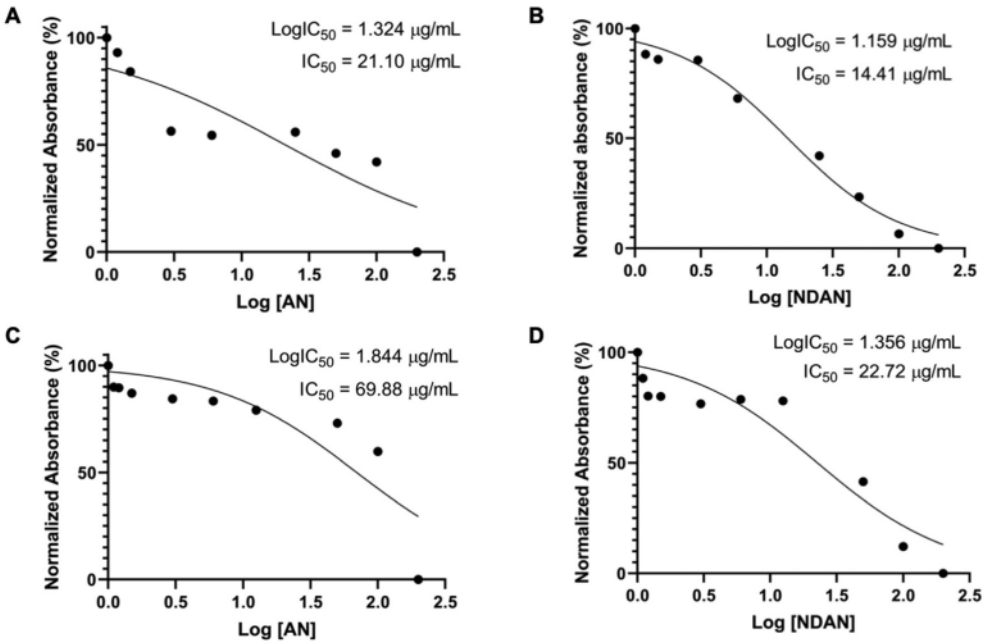

Figure 3. IC_{50} of free annonacin and annonacin coupled with nanodiamond in MCF7 (A–B) and T47D cells (C–D).

significantly ($P < 0.05$) increased the percentage of cells exhibiting positive caspase-3 staining compared to that in the CTL(-) group (Figure 10). The percentage of cells positive for caspase-3 staining was not significantly different between the AN and NDAN groups. The caspase-3 positive cells in the NDAN group were not statistically significant compared to those in the NC group, while in the AN group, the number of caspase-3 positive cells were significantly ($P < 0.05$) different compared to those in the NC group. Mammary ductal epithelium measurements suggested that administration of annonacin coupled with nanodiamonds significantly ($P < 0.05$) reduced the thickness of mammary ductal epithelium in breast cancer-induced rats compared to that in the CTL(-) group. The thickness of the mammary ductal epithelium in the NDAN group was significantly different from that in the AN group ($P < 0.05$) (Figure 11).

4. Discussion

Cancer is a serious disease that is on the increase in both developed and developing countries (DeSantis et al., 2019; Ngulde et al., 2020). The most commonly used cancer treatment methods are surgery, radiotherapy, and chemotherapy (DeMartel et al., 2012). However, conventional cancer therapies have low viability and induce intrinsic toxicity

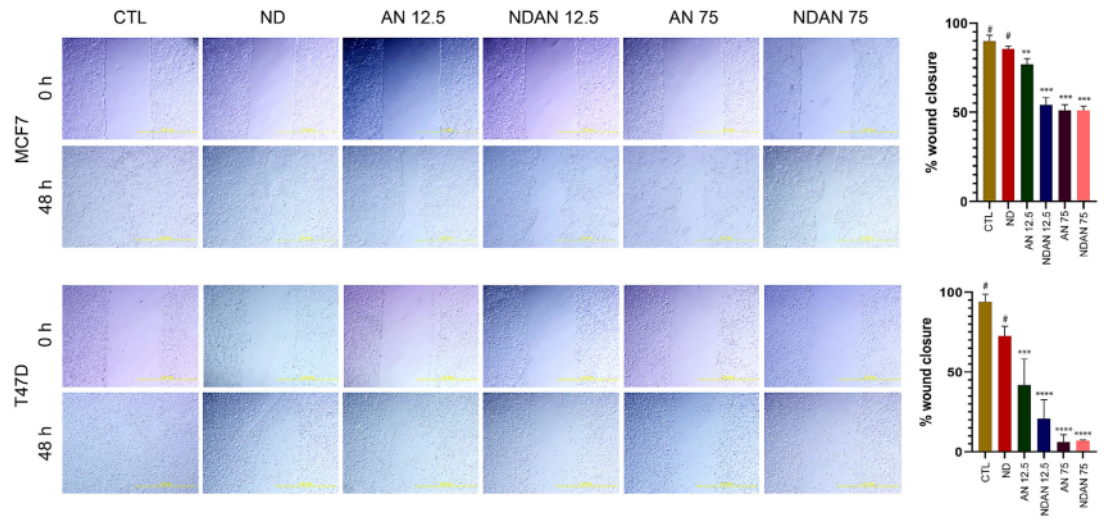

Figure 4. Cell migration assay of MCF-7 and T47D cells administered with 12.5 and 75 μg/mL of annonacin coupled with nanodiamond for 48 h. Mean values with the different signs are significantly different compared to the control group.

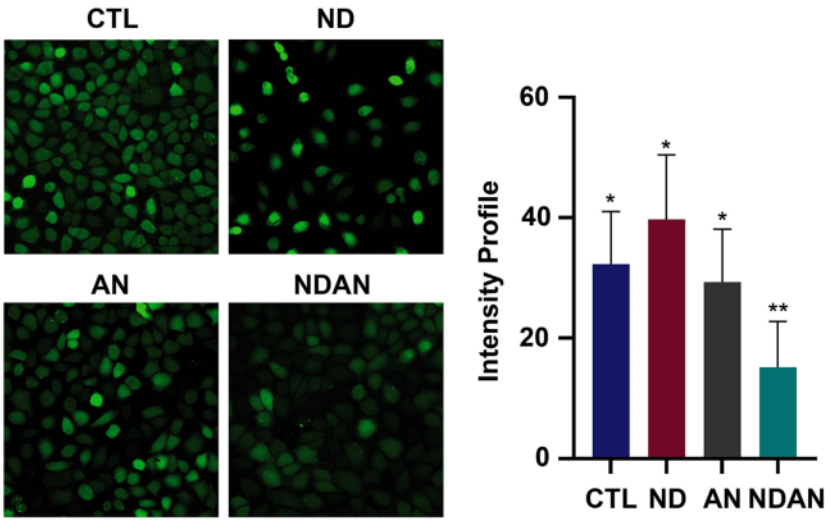

Figure 5. The ROS level in MCF-7 cells administered with 12.5 μg/mL of annonacin coupled with nanodiamond for 24 h. Mean values with the different signs are significantly different at $P < 0.05$.

(Landeros-Martinez et al., 2016). Chemotherapy is a cancer treatment that uses cytotoxic agents to kill cancer cells; however, owing to its non-specificity, it can also kill normal cells during the process. Consequently, it can cause several side effects during and after therapy. Recently, researchers have focused on developing methods that can selectively target cancer cells. Owing to the abnormal structure of blood vessels in tumors, the use of drug delivery systems is expected to be a means to kill cancer cells without affecting normal cells. In this study, we investigated the potency of annonacin, a bioactive compound of *Annona muricata,* as an anti-cancer agent and explored its potential as a carrier for annonacin.

A nanodiamond (ND) is a carbon-based nanoparticle with a high chemical surface biocompatibility that can be used in drug delivery systems. Previously, several studies have reported the potential of nanodiamonds as a carrier of plant bioactive compounds including ciproten, quercetin, and curcumin for cancer therapy (Gismondi et al., 2015; Du et al., 2021). Pharmacokinetic data have shown that annonacin has low viability (Chan et al., 2019). A previous study suggested that supramolecular polymer micelles (SMPM) as a carrier for annonacin could increase the bioavailability of annonacin (Gutierrez et al., 2020). In this study, the annonacin was coupled into nanodiamond and showed an average size of 150–300 nm. The FT-IR spectra of NDAN display the characteristic feature of nanodiamond and annonacin, indicating that the coupling of annonacin to the nanodiamond surface did not alter the nanodiamond structure. To interact with cells and for controlled electrostatic interactions with target sorbent molecules, the zeta potential value is crucial (surfaces of cell membranes are negatively charged) (Shenderova and McGuire, 2015). The complex of annonacin nanodiamond showed negative zeta potential (-65.8 ± 0.1 mV), which is higher than nanodiamond. Electrostatic repulsion forces between the particles increased, corresponding to the zeta

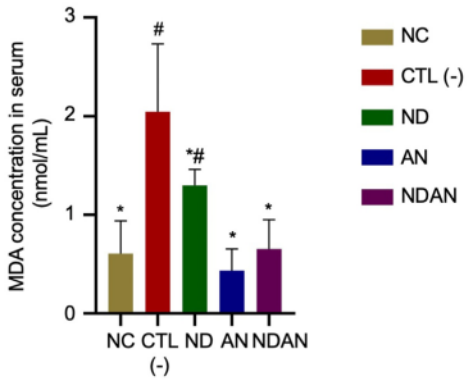

Figure 6. The serum levels of MDA in breast cancer-induced rats following treatment with 17.5 mg/kg body weight of annonacin coupled with nanodiamond for 5 weeks. Mean values with the different signs are significantly different at $P < 0.05$. Each bar represents mean ± SD (n = 5).

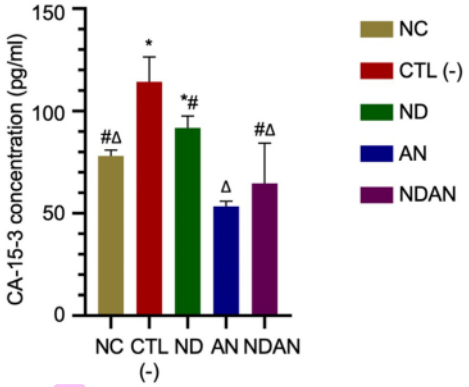

Figure 8. The serum levels of CA-15-3 in breast cancer-induced rats following treatment with 17.5 mg/kg body weight of annonacin coupled with nanodiamond for 5 weeks. Mean values with the different signs are significantly different at $P < 0.05$. Each bar represents mean ± SD (n = 5).

potential. This repulsion reduces the aggregation/flocculation caused by van der Waals interactions by increasing the spacing between the suspended particles. However, because nanoparticles have a lower zeta potential, they tend to aggregate and grow in size (Wang et al., 2014). Moreover, the nanodiamond complex stability study was conducted by incubating it in different media, DMEM, 10% FBS, and complete DMEM. The stable colloidal suspension system that inhibits nanoparticle aggregation is thought to consist of nanoparticles with zeta potentials greater than or equal to +30 mV or less than -30 mV (Honary and Zahir, 2013). The zeta potential value of the annonacin nanodiamond complex varied between -67.4 mV and -58.6 mV on different mediums, showing that it remained stable.

Another study reported antiproliferative effects of annonacin on endometrial cancer cells (Yap et al., 2017). In addition, one more study reported the potency of annonacin in inducing cell cycle arrest and apoptosis of MCF7 cells in the estrogen receptor-related pathways (Ko et al., 2011). To the best of our knowledge, this is the first study to report the potency of nanodiamonds that can be used as a carrier of annonacin to increase its viability, thus increasing its effect on MCF7 cell viability (Figure 2). Twenty-four hours after treatment, the cell viability of the group treated with annonacin coated onto nanodiamonds was significantly lower than that of the group treated with annonacin only.

Elevated ROS levels have been observed in almost all types of cancers. Elevated ROS levels can promote tumor development and metastasis. Therapeutic antioxidants may prevent early processes in carcinogenesis that is caused by ROS. High ROS levels in cancer cells can result from several cell activities or signaling pathways, including increased metabolic activity and oncogene activity (Liou and Storz, 2010; Szatrowski and Nathan, 1991). A previous study reported that crude *A. muricata* leaf extract can trigger intrinsic apoptotic pathways through ROS formation in breast cancer cells (Kim et al., 2018). In this study, we showed that annonacin, a bioactive compound of *A. muricata*, can reduce ROS and MDA levels in MCF7 cells and breast cancer-induced rats, and annonacin coated onto nanodiamonds can reduce the level of ROS even further (Figures 3 and 4).

ROS-sensitive signaling pathways are constantly activated in many types of cancers, wherein they are involved in cell proliferation, cell survival, and inflammation (Storz, 2005). Several signaling pathways are regulated by ROS, including the mitogen-activated protein (MAP) kinase/ERK cascade, nuclear factor κB (NFκB), and PI3K/Akt pathways. In cancer cells, activation of the PI3K/Akt signaling pathway inactivates the TP53 tumor-suppressor gene, which is a common mechanism to promote proliferation and escape from apoptotic cell death. Activation of PI3K/Akt signaling mediates a negative control of p53 levels by

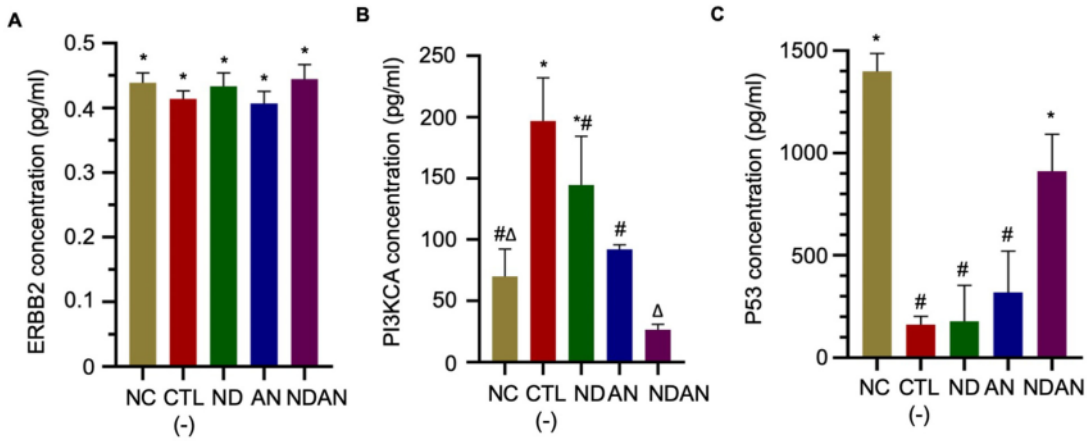

Figure 7. The ERBB2, PI3KCA, and P53 expression in breast cancer-induced rats following treatment with 17.5 mg/kg body weight of annonacin coupled with nanodiamond for 5 weeks. Mean values with the different signs are significantly different at $P < 0.05$. Each bar represents mean ± SD (n = 5).

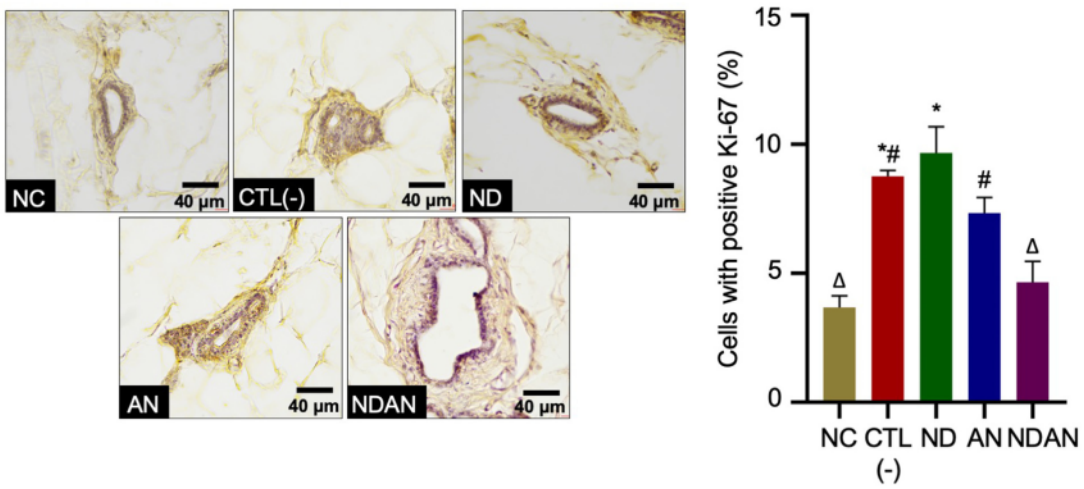

Figure 9. Cells with positive Ki-67 staining in breast cancer-induced rats following treatment with 17.5 mg/kg body weight of annonacin coupled with nanodiamond for 5 weeks (Scale bar: 40 μm). Mean values with the different signs are significantly different at $P < 0.05$. Each bar represents mean ± SD (n = 5).

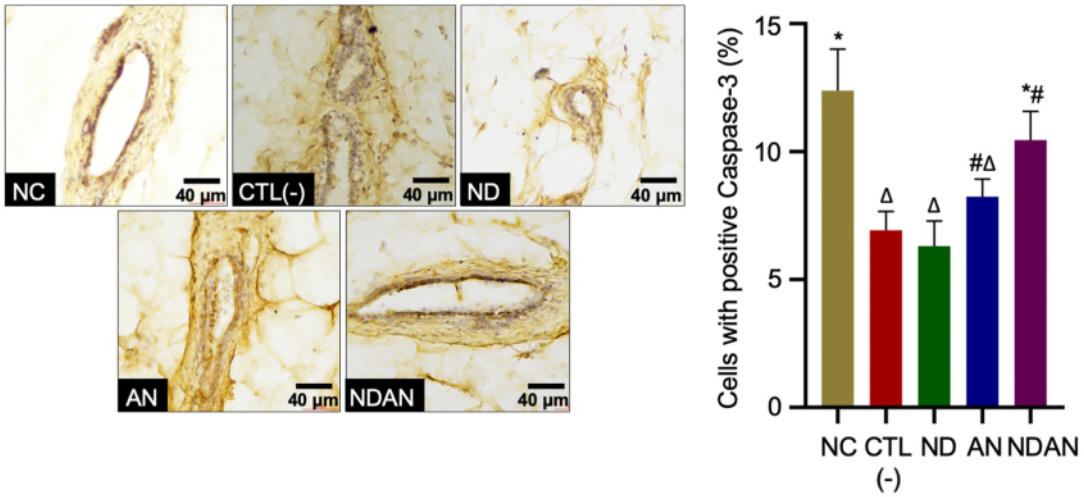

Figure 10. Cells with positive Caspase-3 staining in breast cancer-induced rats following treatment with 17.5 mg/kg body weight of annonacin coupled with nanodiamond for 5 weeks (Scale bar: 40 μm). Mean values with the different signs are significantly different at $P < 0.05$. Each bar represents mean ± SD (n = 5).

enhancing MDM2 (murine double minute 2)-mediated targeting of p35 for degradation (Abraham & O'Neill, 2014; Liu et al., 2020). In this study, we showed that annonacin affects the PI3K signaling pathway by downregulating PI3KCA expression, thus increasing p53 expression. Treatment of a rat model with annonacin coated onto nanodiamonds decreased PI3KCA levels and increased p53 expression even further, suggesting the ability of nanodiamonds to act as a carrier to increase annonacin activity. A previous study reported that annonacin exerts a cytotoxic effect by inhibiting mitochondrial complex I, thus leading to the repression of ubiquinone-linked NADH oxidase (Md-Roduan, 2019).

We examined the expression of CA-15-3 in the serum of rats. Cancer antigen 15–3 (CA-15-3) is an antigen encoded by the MUC1 gene, which is expressed on the surface of benign and malignant epithelial cells. The serum level of CA-15-3 is used as a marker to monitor metastasis in patients with breast cancer (Prabasheela and Arivazhagan, 2011; Hashim, 2013; Keshaviah et al., 2007). In our study, the serum level of CA-15-3 increased in the negative control group and decreased significantly when annonacin was administered. This result can be used as preliminary data to study the potential effect of annonacin in preventing breast cancer metastasis. Further studies are needed to explore more metastatic markers, including carcinoembryonic antigen (CEA), matrix metalloproteinase (MMP)-2, and MMP9.

Ki-67 and caspase-3 proteins are two important prognostic variables for breast cancer. The rate of tumor proliferation is one of the most important prognostic factors in breast cancer that is commonly detected by immunohistochemical staining of Ki-67. Ki-67 is an easily used proliferation marker and a reliable substitute for mitotic counts (Zhang et al., 2010). Several studies have investigated the significance of the Ki-67 proliferation index, which is significantly higher in malignant breast cancers than in benign tumors (De Azambuja et al., 2007). In our study, the administration of annonacin coupled with nanodiamonds significantly reduced the percentage of cells positive for Ki-67 staining.

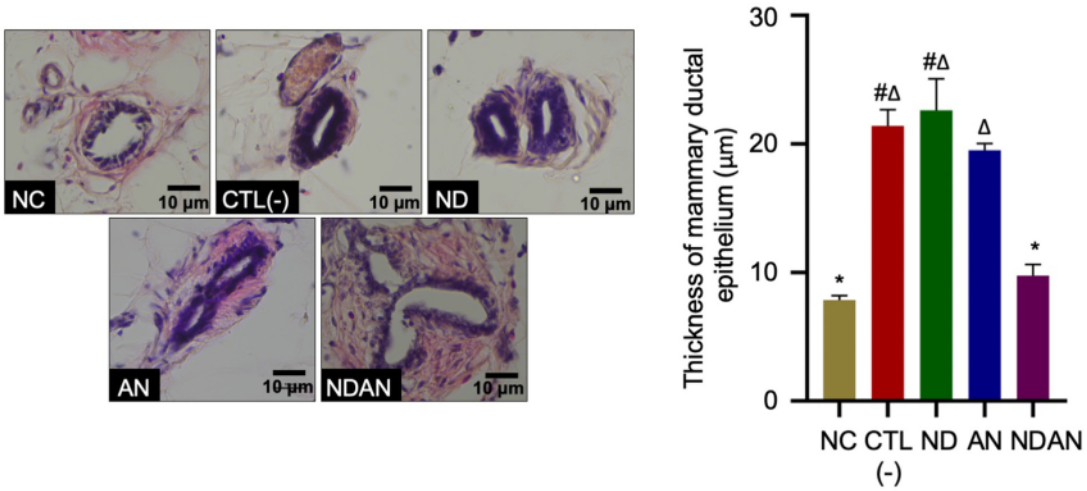

Figure 11. The thickness of mammary ductal epithelium in breast cancer-induced rats following treatment with 17.5 mg/kg body weight of annonacin coupled with nanodiamond for 5 weeks (Scale bar: 10 μm). Mean values with the different signs are significantly different at $P < 0.05$. Each bar represents mean ± SD ($n = 5$).

Furthermore, the conjugation of annonacin with nanodiamonds significantly increased the anti-cancer properties of annonacin, as shown by a significant reduction in the percentage of cells showing Ki-67 staining in NDAN group than in AN group.

A balance between apoptosis and cell proliferation determines tumor growth (Chang et al., 2000). Caspase-3 is classified as an executioner caspase, and is commonly used as a marker for apoptosis in cancer. Administration of annonacin coupled with nanodiamonds significantly reduced the percentage of cells showing positive caspase-3 staining, thereby suggesting the ability of annonacin to induce apoptosis in cancer cells as well as the efficacy of nanodiamonds as a carrier of annonacin. Finally, we examined the thickness of the mammary ductal epithelium in breast cancer-induced rats. The reduction of cancer cell proliferation and increased cancer cell apoptosis resulted in a reduction in the thickness of the mammary ductal epithelium. Administration of annonacin coupled with nanodiamonds significantly reduced the thickness of the mammary ductal epithelium, and conjugation of annonacin with nanodiamonds significantly increased its anti-cancer activity, as shown by the significant reduction in mammary ductal epithelium in the group treated with annonacin coupled with nanodiamonds than in the group treated with annonacin only (Figure 11). A recent study reported that conjugation with nanodiamonds can increase vascular leakage, thus allowing a higher amount of drug to enter the tumor microenvironment (Setyawati et al., 2016).

5. Conclusions

Collectively, this study demonstrates the novel potential of nanodiamonds as a carrier of annonacin. In addition, we demonstrated a novel mechanism achieved by annonacin in breast cancer cells that involves the PI3K/Akt signaling pathway. Future clinical investigations should explore the mechanisms by which annonacin contributes to the prevention of metastasis in breast cancer cells.

Declarations

Author contribution statement

Firli Rahmah Primula Dewi: Conceived and designed the experiments; Performed the experiments; Analyzed and interpreted the data; Wrote the paper.

Nadia Shoukat; A'liyatur Rosyidah: Performed the experiments; Wrote the paper.

Na'ilah Insani Alifiyah: Performed the experiments; Analyzed and interpreted the data; Wrote the paper.

Muhammad Darwin Prenggono; Hartono; Sri Puji Astuti Wahyuningsih: Contributed reagents, materials, analysis tools or data.

Funding statement

This work was supported by Hibah Riset Mandat Dosen Muda, Universitas Airlangga, Indonesia (grant number: 390/UN3.14/PT/2020) to Dr. Firli Rahmah Primula Dewi.

Data availability statement

Data included in article/supp. material/referenced in article.

Declaration of interest's statement

The authors declare no conflict of interest.

Additional information

Supplementary content related to this article has been published online at https://doi.org/10.1016/j.heliyon.2022.e11418.

References

Abd-Rabou, A.A., Abdalla, A.M., Ali, N.A., et al., 2017. *Moringa oleifera* root induces cancer apoptosis more effectively than leave nanocomposites and its free counterpart. Asian Pac. J. Cancer Prev. APJCP 18, 2141–2149.

Abraham, A.G., O'Neill, E., 2014. PI3K/Akt-mediated regulation of p53 in cancer. Biochem. Soc. Trans. 42, 798–803.

Burdick, A.D., Davis, J.W., Liu, K.J., Hudson, L.G., Shi, H., Monske, M.L., Burchiel, S.W., 2003. Benzo(a)pyrene quinones increase cell proliferation, generate reactive oxygen species, and transactivate the epidermal growth factor receptor in breast epithelial cells. Cancer Res. 63, 7825–7833.

Chan, W.J., McLachlan, A.J., Hanrahan, J.R., et al., 2019. The safety and tolerability of *Annona muricata* leaf extract: a systematic review. J. Pharm. Pharmacol. 72, 1–16.

Chang, J., Ormerod, M., Powles, T.J., Allred, D.C., Ashley, S.E., Dowsett, M., 2000. Apoptosis and proliferation as predictors of chemotherapy response in patients with breast carcinoma. Cancer 89, 2145–2152.

Chauhan, S., Jain, N., Nagaich, U., 2020. Nanodiamonds with powerful ability for drug delivery and biomedical applications: recent updates on in vivo study and patents. J. Pharm. Anal. 10, 1–12.

Chow, E.K., Zhang, X.Q., Chen, M., et al., 2011. Nanodiamond therapeutic delivery agents mediate enhanced chemoresistant tumor treatment. Sci. Transl. Med. 3, 73ra21.
Coughlin, S.S., 2018. Oxidative stress, antioxidants, physical activity, and the prevention of breast cancer initiation and progression. J. Environ. Health Sci. 4, 55–57.
De Azambuja, E., Cardoso, F., de Castro Jr., G., Colozza, M., Mano, M.S., Durbecq, V., Sotiriou, C., Larsimont, D., Piccart-Gebhart, M.J., Paesmans, M., 2007. Ki-67 as prognostic marker in early breast cancer: a meta-analysis of published studies involving 12,155 patients. Br. J. Cancer 21, 1504–1513.
DeMartel, C., Ferlay, J., Franceschi, S., et al., 2012. Global burden of cancers attributable to infections in 2008: a review and synthetic analysis. Lancet Oncol. 13, 607–615.
DeSantis, C.E., Jiemin, M., Mia, M.G., et al., 2019. Breast cancer statistics 2019. CA. CA Cancer J. Clin 69, 438–451.
Dewi, F.R.P., Jiapaer, S., Kobayashi, A., et al., 2021. Nucleoporin TPR (translocated promoter region, nuclear basket protein) upregulation alters MTOR-HSF1 trails and suppresses autophagy induction in ependymoma. Autophagy 17, 1001–1012.
Du, B.W., Tien, L.T., Lin, C.C., Ko, F.H., 2021. Use of curcumin-modified diamond nanoparticles in cellular imaging and the distinct ratiometric detection of Mg^{2+}/Mn^{2+} ions. Nanoscale Adv. 3, 4459–4470.
El-Say, K.M., 2011. Nanodiamond as a drug delivery system: applications and prospective. J. Appl. Pharmaceut. Sci. 1, 29–39.
Gismondi, A., Reina, G., Orlanducci, S., Mizzoni, F., Gay, S., Terranova, M.L., Canini, A., 2015. Nanodiamonds coupled with plant bioactive metabolites: a nanotech approach for cancer therapy. Biomaterials 38, 22–35.
Gutiérrez, M.T., Durán, A.G., Mejías, F.J.R., Molinillo, J.M.G., Megías, D., Valdivia, M.M., Macías, F.A., 2020. Bio-guided isolation of acetogenins from *Annona cherimola* deciduous leaves: production of nanocarriers to boost the bioavailability properties. Molecules 25, 4861.
Hashim, Z.M., 2013. The significance of CA 15-3 in breast cancer patients and its relationship to HER-2 receptor status. Int. J. Immunopathol. Pharmacol. 27, 45–51.
Hemelaar, S.R., Nagl, A., Bigot, F., Rodríguez-García, M.M., de Vries, M.P., et al., 2017. The interaction of fluorescent nanodiamond probes with cellular media. Microchimica Acta 184 (4), 1001–1009.
Honary, S., Zahir, F., 2013. Effect of zeta potential on the properties of nano-drug delivery systems – a review. Trop. J. Pharmaceut. Res. 12 (2), 256–273.
Keshaviah, A., Dellapasqua, S., Rotmensz, N., et al., 2007. CA15-3 and alkaline phosphatase as predictors for breast cancer recurrence: a combined analysis of seven International Breast Cancer Study Group trials. Ann. Oncol. 18, 701–708.
Kim, J.Y., Dao, T.T.P., Song, K., et al., 2018. Annona muricata Leaf Extract Triggered Intrinsic Apoptotic Pathway to Attenuate Cancerous Features of Triple Negative Breast Cancer MDA-MB-231 Cells. Evid Based Complement Alternat. Med., 7972916
Ko, Y.M., Wu, T.Y., Wu, Y.C., et al., 2011. Annonacin induces cell cycle-dependent growth arrest and apoptosis in estrogen receptor-α-related pathways in MCF-7 cells. J. Ethnopharmacol. 137, 1283–1290.
Landeros-Martinez, L.L., Chavez-Flores, D., Orrantia-Borunda, E., et al., 2016. Construction of a nanodiamond–tamoxifen complex as a breast cancer drug delivery vehicle. J. Nanomater. 2016, 1–9, 682105.
Liou, G.Y., Storz, P., 2010. Reactive oxygen species in cancer. Free Radic. Res. 44 (5).
Liu, K., Xue, B., Bai, G., et al., 2020. F-box protein FBXO31 modulates apoptosis and epithelial-mesenchymal transition of cervical cancer via inactivation of the PI3K/AKT-mediated MDM2/p53 axis. Life Sci. 15.
Md-Roduan, M.R., Hamid, R.A., Mohtarrudin, N., 2019. Modulation of cancer signalling pathway(s) in two-stage mouse skin tumorigenesis by annonacin. BMC Compl. Alternative Med. 19, 1–16.
Ngulde, S.I., Sandabe, U.K., Abounader, R., et al., 2020. Activities of some medicinal plants on the proliferation and invasion of brain tumor cell lines. Adv Pharmacol Pharmaceut. Sci., 3626879
Park, S.A., Na, H.K., Kim, E.H., Cha, Y.N., Surg, Y.J., 2009. 4-hydroxyestradiol induces anchorage-independent growth of human mammary epithelial cells via activation of IkappaB kinase: potential role of reactive oxygen species. Cancer Res. 69, 2416–2424.
Petit, T., Puskar, L., 2018. FTIR spectroscopy of nanodiamonds: methods and interpretation. Diam. Relat. Mater. 89, 52–66.
Prabasheela, B., Arivazhagan, R., 2011. CA-15-3 and breast cancer. Int. J. Pharma Bio Sci. 2, 34–38.
Qazi, A.K., Siddiqui, J.A., Jahan, R., Chaudhary, S., Walker, L.A., et al., 2018. Emerging therapeutic potential of graviola and its constituents in cancers. Carcinogenesis 39 (4), 522–533.
Roy, U., Drozd, V., Durygin, A., et al., 2018. Characterization of nanodiamond-based anti-HIV drug delivery to the brain. Sci. Rep. 8, 1–12.
Setyawati, M.I., Mochalin, V.N., Leong, D.T., 2016. Tuning endothelial permeability with functionalized nanodiamonds. ACS Nano 10, 1170–1181.
Shenderova, O., McGuire, G.E., 2015. Science and engineerung of nanodiamond particle surfaces for biological applications. Biointerphase 10 (3), 030802.
Siegel, R.L., Miller, K.D., Fuchs, H.E., Jemal, A., 2021. Cancer statistics, 2021. CA. CA Cancer J. Clin. 71, 7–33.
Storz, P., 2005. Reactive oxygen species in tumor progression. Front. Biosci. 10, 1881–1896.
Szatrowski, T.P., Nathan, C.F., 1991. Production of large amounts of hydrogen peroxide by human tumor cells. Cancer Res. 51, 794–798.
Tsai, L.W., Lin, Y.C., Perevedentseva, E., et al., 2016. Nanodiamonds for medical applications: interaction with blood in vitro and in vivo. Int. J. Mol. Sci. 17, 5–9.
Wahab, A.,S.M., Jantan, I., Haque, M.A., Arshad, L., 2018. Exploring the leaves of Annona muricata L. As a source of potential anti-inflammatory and anticancer agents. Front. Pharmacol. 9, 1–20.
Wang, X., Low, X.C., Hou, W., Abdullah, L.N., Toh, T.B., et al., 2014. Epirubicin-adsorbed nanodiamonds stem cells. ACS Nano 12, 12151–12166.
Wei, S., Li, L., Du, X., Li, Y., 2019. Off-On nanodiamond drug platform for targeted cancer imaging and therapy. J. Mater. Chem. B 7, 3390–3402.
Yap, C.V., Kavita, S.S., Sik, W.K., et al., 2017. Annonacin exerts antitumor activity through induction of apoptosis and extracellular signal-regulated kinase inhibition. Pharmacogn. Res. 9, 378–383.
Yuan, S.S.F., Hsueh-Ling, C., Hsiao-Wen, C., Yao-Tsung, Y., Ying-Hsien, K., Kuei-Hsiang, L., Yang-Chang, W., Jinu-Huang, S., 2003. Annonacin, a mono-tetrahydrofuran acetogenin, arrests cancer cells at the G1 phase and causes cytotoxicity in a Bax- and caspase-3-related pathway. Life Sci. 72, 2853–2861.
Zhang, R., Chen, H.J., Wei, B., Zhang, H.Y., Pang, Z.G., Zhu, H., Zhang, Z., Fu, J., Bu, H., 2010. Reproducibility of the Nottingham modification of the Scarff-Bloom-Richardson histological grading system and the complementary value of Ki-67 to this system. Chin. Med. J. 5, 1976–1982.

Increasing the effect of annonacin using nanodiamonds to inhibit breast cancer cells growth in rats (Rattus norvegicus)-Induced breast cancer

ORIGINALITY REPORT

11%	9%	6%	2%
SIMILARITY INDEX	INTERNET SOURCES	PUBLICATIONS	STUDENT PAPERS

PRIMARY SOURCES

1	estramps.pangea.org Internet Source	<1%
2	qascf.com Internet Source	<1%
3	www.fn-test.com Internet Source	<1%
4	www.medicalnewstoday.com Internet Source	<1%
5	www.japtr.org Internet Source	<1%
6	A. Taniguchi. "The Effects of LAMP1 and LAMP3 on M180 Amelogenin Uptake, Localization and Amelogenin mRNA Induction by Amelogenin Protein", Journal of Biochemistry, 06/16/2008 Publication	<1%
7	opus.lib.uts.edu.au Internet Source	<1%

8	qu.edu.iq Internet Source	<1 %
9	spandidos-publications.com Internet Source	<1 %
10	www.bioseek.eu Internet Source	<1 %
11	www.turkjps.org Internet Source	<1 %
12	doaj.org Internet Source	<1 %
13	jnanobiotechnology.biomedcentral.com Internet Source	<1 %
14	faksignaling.com Internet Source	<1 %
15	search.bvsalud.org Internet Source	<1 %
16	www.pakbs.org Internet Source	<1 %
17	Submitted to National Institute of Pharmaceutical Education and Research Student Paper	<1 %
18	citeseerx.ist.psu.edu Internet Source	<1 %
19	mdpi.com Internet Source	

		<1%
20	pubs.aip.org Internet Source	<1%
21	www.sid.ir Internet Source	<1%
22	dehydrogenase-signal.com Internet Source	<1%
23	epdf.tips Internet Source	<1%
24	eprints.utar.edu.my Internet Source	<1%
25	storage.googleapis.com Internet Source	<1%
26	www.journalajst.com Internet Source	<1%
27	Becuwe, Philippe, Marie Ennen, Rémi Klotz, Claire Barbieux, and Stéphanie Grandemange. "Manganese superoxide dismutase in breast cancer: From molecular mechanisms of gene regulation to biological and clinical significance", Free Radical Biology and Medicine, 2014. Publication	<1%

28	Mutlu, Esra, Yo-Chan Jeong, Leonard B. Collins, Amy-Joan L. Ham, Patricia B. Upton, Gary Hatch, Darrell Winsett, Paul Evansky, and James A. Swenberg. "A New LC-MS/MS Method for the Quantification of Endogenous and Vinyl Chloride-Induced 7-(2-Oxoethyl)Guanine in Sprague–Dawley Rats", Chemical Research in Toxicology, 2012. Publication	<1 %
29	ediss.uni-goettingen.de Internet Source	<1 %
30	sjce.journals.sharif.edu Internet Source	<1 %
31	www.ndsl.kr Internet Source	<1 %
32	Submitted to Western Illinois University Student Paper	<1 %
33	eprints.nottingham.ac.uk Internet Source	<1 %
34	fungalbiolbiotech.biomedcentral.com Internet Source	<1 %
35	researchmgt.monash.edu Internet Source	<1 %
36	www.mattioli1885journals.com Internet Source	<1 %

37	www.omicsonline.org Internet Source	<1%
38	"Poster presentations, P1-P263", European Journal of Nuclear Medicine and Molecular Imaging, 2005 Publication	<1%
39	Feras Brrow, Chadi Soukkarieh, Alaa Salman, Sophie Barguil. "Evaluation of the cytotoxicity of nickel chloride and nickel nitrate on HEK293T cell line", Research Square Platform LLC, 2023 Publication	<1%
40	Li Volti, G., T. Musumeci, R. Pignatello, P. Murabito, I. Barbagallo, C. Carbone, A. Gullo, and G. Puglisi. "Antioxidant potential of different melatonin-loaded nanomedicines in an experimental model of sepsis", Experimental Biology and Medicine, 2012. Publication	<1%
41	Xiuren Zhang. "Tomato is a highly effective vehicle for expression and oral immunization with Norwalk virus capsid protein", Plant Biotechnology Journal, 7/2006 Publication	<1%
42	Yolande I. Openda, Bokolombe P. Ngoy, Tebello Nyokong. "Photodynamic Antimicrobial Action of Asymmetrical	<1%

Porphyrins Functionalized Silver-Detonation Nanodiamonds Nanoplatforms for the Suppression of Staphylococcus aureus Planktonic Cells and Biofilms", Frontiers in Chemistry, 2021
Publication

43	Yuanhui Song, Azmeer Sharipol, Hitoshi Uchida, Matthew H. Ingalls et al. "Encapsulation of Primary Salivary Gland Acinar Cell Clusters and Intercalated Ducts (AIDUCs) within Matrix Metalloproteinase (MMP) - Degradable Hydrogels to Maintain Tissue Structure and Function", Advanced Healthcare Materials, 2022 Publication	<1 %
44	cris.maastrichtuniversity.nl Internet Source	<1 %
45	s-space.snu.ac.kr Internet Source	<1 %
46	stm.sciencemag.org Internet Source	<1 %
47	www.zhb.uni-luebeck.de Internet Source	<1 %
48	A Cardillo. "Factors that predict early treatment failure for patients with locally advanced (T4) breast cancer", British Journal of Cancer, 06/03/2008	<1 %

Publication

49	Aamir Ahmad. "Role of Novel Nutraceuticals Garcinol, Plumbagin and Mangiferin in the Prevention and Therapy of Human Malignancies: Mechanisms of Anticancer Activity", Nutraceuticals and Cancer, 2012 Publication	<1 %
50	Cipres, A.. "Abl functions as a negative regulator of Met-induced cell motility via phosphorylation of the adapter protein CrkII", Cellular Signalling, 200708 Publication	<1 %
51	Fang Li, Yuqiong Yan, Jiqiang Guo, Chongzhi Bai. "CD147 promotes breast cancer invasion and metastasis by inducing EMT and upregulating MMPs via the MAPK/ERK signaling pathway", Research Square Platform LLC, 2023 Publication	<1 %
52	H. L. McAlroy, D. L. Bovell, J. A. Plumb, P. Thompson, S. M. Wilson. " Drug Extrusion, I Efflux and the Control of Intracellular [Ca] in Drug-Resistant Ovarian Epithelial Cells ", Experimental Physiology, 1999 Publication	<1 %
53	Islamic Azad University–Isfahan Branch Publication	<1 %

54 Mrklić, Ivana, Vesna Ćapkun, Zenon Pogorelić, and Snježana Tomić. "Prognostic value of Ki-67 proliferating index in triple negative breast carcinomas", Pathology - Research and Practice, 2013.
Publication
<1%

55 Sinha, Sonam, Samriddhi Shukla, Sajid Khan, Trygve O. Tollefsbol, and Syed M. Meeran. "Epigenetic reactivation of p21CIP1/WAF1 and KLOTHO by a combination of bioactive dietary supplements is partially ERα-dependent in ERα-negative human breast cancer cells", Molecular and Cellular Endocrinology, 2015.
Publication
<1%

56 Sushreesangita P. Behera, Rajiv K. Saxena. "Nanodiamonds inhibit scratch-wound repair in lung epithelial cell monolayers by blocking cell migration and inhibiting cell proliferation", Toxicology Letters, 2021
Publication
<1%

57 Wenhui Yi, Asif Khalid, Naila Arshad, M. Sohail Asghar et al. "Recent Progress and Perspective of an Evolving Carbon Family From 0D to 3D: Synthesis, Biomedical Applications, and Potential Challenges", ACS Applied Bio Materials, 2023
Publication
<1%

ar.iiarjournals.org

58	Internet Source	<1%
59	doi.org Internet Source	<1%
60	doras.dcu.ie Internet Source	<1%
61	epublications.uef.fi Internet Source	<1%
62	flex.flinders.edu.au Internet Source	<1%
63	jebas.org Internet Source	<1%
64	lra.le.ac.uk Internet Source	<1%
65	nemertes.lis.upatras.gr Internet Source	<1%
66	nphs.kmu.edu.tw Internet Source	<1%
67	ouci.dntb.gov.ua Internet Source	<1%
68	pure.uva.nl Internet Source	<1%
69	refubium.fu-berlin.de Internet Source	<1%

70	rosdok.uni-rostock.de Internet Source	<1%
71	scholarworks.gsu.edu Internet Source	<1%
72	ueaeprints.uea.ac.uk Internet Source	<1%
73	www.amedeo.com Internet Source	<1%
74	www.degruyter.com Internet Source	<1%
75	"Nanocarriers: Drug Delivery System", Springer Science and Business Media LLC, 2021 Publication	<1%

Exclude quotes	On	Exclude matches	Off
Exclude bibliography	On		

Increasing the effect of annonacin using nanodiamonds to inhibit breast cancer cells growth in rats (Rattus norvegicus)-Induced breast cancer

GRADEMARK REPORT

FINAL GRADE

/0

GENERAL COMMENTS

Instructor

PAGE 1

PAGE 2

PAGE 3

PAGE 4

PAGE 5

PAGE 6

PAGE 7

PAGE 8

PAGE 9

PAGE 10

PAGE 11